THE ASTROPHYSICAL JOURNAL, 441:170–181, 1995 March 1

NON-LTE SPECTRAL ANALYSIS AND MODEL CONSTRAINTS ON SN 1993J

E. BARON,[1] P. H. HAUSCHILDT,[2] D. BRANCH,[1] S. AUSTIN,[2] P. GARNAVICH,[3] HONG BAE ANN,[3,4]
R. M. WAGNER,[5] A. V. FILIPPENKO,[6] T. MATHESON,[6] AND JAMES LIEBERT[7]
Received 1994 June 8; accepted 1994 September 9

ABSTRACT

We present non-LTE synthetic spectra for a time series of observations of SN 1993J obtained on 1993 March 30–31, April 7, April 13–15, and June 13 UT. The spectra are dominated by hydrogen Balmer lines; neutral helium lines, which have been nonthermally excited; and Fe II features. The density profile evolves from an extremely steep "brick wall" structure with an equivalent power-law index of about 50 on March 30 to a more typical SN II profile with a power law index of about 10. The early spectra are well fitted by a solar composition of metals, although an enhanced abundance of helium is required in order to fit the neutral helium lines. By June 13, the photosphere has receded deep into the helium layer, although there appears to be a layer of hydrogen at higher velocity.

The distance is estimated for each epoch. While consistent results are found for spectra obtained in the month of April, the spread in distances from March to June is quite large. Our value for April is $\mu = 28.0 \pm 0.3$ mag, consistent with the recent Cepheid distance to the host galaxy M81. We also compare our results to other implementations of the expanding photosphere method.

Subject headings: galaxies: distances and redshifts — galaxies: individual (M81) — supernovae: individual (SN 1993J)

1. INTRODUCTION

SN 1993J was the brightest supernova since SN 1987A, and even though it was about 70 times more distant than SN 1987A, the higher luminosity and convenient location in the northern hemisphere have led to considerable interest in this object. SN 1993J, like SN 1987A, was a Type II supernova showing strong Balmer lines in its spectra. Also like SN 1987A, the light curve of SN 1993J was anomalous (e.g., Richmond et al. 1994), showing a rapid decline from maximum followed by a secondary rise, powered by the radioactive decay of ^{56}Ni. In addition, about 26 days after explosion, the spectra of SN 1993J began to deviate significantly from those of typical Type II supernovae, in that the Hα emission profile showed a "double-peaked" structure that was due to the effects of the He I λ6678 line (Hu et al. 1993; Filippenko & Matheson 1993; Filippenko, Matheson, & Ho 1993). Thus, SN 1993J well deserves the classification Type IIpec.

The behavior of the light curve and spectra are understood to be the result of the explosion of an extended (i.e., red giant–sized) star with a low hydrogen envelope mass. Hydrogen envelope masses in the range $\approx$0.1–0.6 $M_\odot$ are inferred (cf. Nomoto et al. 1993; Podsiadlowski et al. 1993; Bartunov et al. 1994; Utrobin 1994; Woosley et al. 1994). Efforts to identify the progenitor suggest a G8–K0 supergiant in an OB association, giving a main-sequence mass of $\sim$17 $M_\odot$ (Aldering, Humphreys, & Richmond, 1994), which corresponds to a helium core mass of about 4–5 $M_\odot$. The total mass ejected should be in the range 2–3.5 $M_\odot$, assuming that a typical mass neutron star was produced in the explosion. The only way to have such large amounts of mass loss is via a binary interaction (Podsiadlowski, Joss, & Hsu 1992), unless the progenitor identification is in error and the progenitor was significantly more massive such that it could lose most of its envelope in a Wolf-Rayet phase (Höflich, Langer, & Duschinger 1993).

In addition to optical and infrared observations, SN 1993J has been observed in the X-ray band by *ASCA*, *ROSAT*, and the OSSE instrument on *CGRO*. The observed X-ray luminosity at 10–20 days is in the range $L = (3\text{–}50) \times 10^{39}$ ergs s^{-1} (Tanaka et al. 1993; Zimmermann et al. 1994; Leising et al. 1994). SN 1993J has also been observed at radio wavelengths; in fact, it is probably the best observed radio supernova to date (Van Dyk et al. 1994; Pooley & Green 1993), and although the observations do not exactly fit a standard Chevalier (1984) model of circumstellar interaction, they can be reconciled with a model where the wind density falls of less steeply than r^{-2}, i.e., in a model where $\dot{M}/v_w$ varies with time, where $\dot{M}$ is the mass loss rate and v_w is the wind velocity (Fransson, Lundquist, & Chevalier 1994).

Our aim in this paper is to examine in detail the time evolution of the optical spectra and relate it to the physical conditions in the supernova. The expanding photosphere method (Baade 1926; Kirshner & Kwan 1974; Branch et al. 1981) is used to derive the distance to SN 1993J. All dates are given in UT.

2. MODELS

2.1. *Model Construction*

In order to extract detailed quantitative information on velocities, densities, temperatures, and compositions, and to constrain theoretical explosion models it is necessary to analyze the supernova spectrum in detail, via synthetic spectral

[1] Department of Physics and Astronomy, University of Oklahoma, 440 West Brooks, Room 131, Norman, OK 73019-0225.
[2] Department of Physics and Astronomy, Arizona State University, Tempe, AZ 85287-1504.
[3] Dominion Astrophysical Observatory, Herzberg Institute of Astrophysics, 5071 West Saanich Road, Victoria, BC, Canada V8X 4M6.
[4] Postal address: Department of Earth Sciences, Pusan National University, Pusan 609-735, Korea.
[5] Department of Astronomy, Ohio State University, Columbus, OH 43210.
[6] Department of Astronomy, University of California, Berkeley, CA 94720-3411.
[7] Steward Observatory, University of Arizona, Tucson, AZ 85721.

modeling. We use the generalized stellar atmosphere code PHOENIX 4.7 to compute our model atmospheres and synthetic spectra for SN 1993J. This is an updated version of the code used for the analysis of the early spectra of Nova Cygni 1992 (Hauschildt et al. 1994), described there and in Baron, Hauschildt, & Branch (1994) and Allard et al. (1994). We give here only a short description.

PHOENIX uses an accelerated Λ-iteration (ALI or operator splitting) method to solve the time-independent, spherically symmetric, *fully* relativistic radiative transfer equation for lines and continua, to all orders in v/c including the effects of relativistic Doppler shift, advection, and aberration (Hauschildt 1992a). The multilevel, non-LTE rate equations can be solved self-consistently for H I (15 levels), He I (11 levels), He II (10 levels), Mg II (three levels), Ca II (five levels), and Na I (three levels), using an ALI method (Rybicki & Hummer 1991; Hauschildt 1993). Simultaneously we solve for the special relativistic condition of radiative equilibrium in the Lagrangian frame (Hauschildt 1992b) using either a partial linearization or a modified Unsöld-Lucy temperature correction scheme. The relativistic effects, in particular the first-order effects of advection and aberration, are important at the high expansion velocities observed in typical SNs (Hauschildt, Best, & Wehrse 1991). We have obtained good convergence for the models presented in this paper; specifically we use the convergence criteria: $\delta F/F < 0.01$ and $\int (\eta - \kappa J) d\lambda / \int \kappa J \, d\lambda < 0.02$ for the radiative equilibrium functions and $\delta N/N < 0.01$ for the non-LTE occupation numbers.

The generalized (for non-LTE) equation of state (EOS) is solved for 40 elements, and up to six ionization stages per element, for a total of 176 species. Only the ions listed in the previous paragraph are treated in non-LTE; for the others the level populations are treated in LTE. Test calculations showed that for the conditions found in SNs at the stage of their spectral evolution we consider here, molecules and negative ions are unimportant and we neglect them with the benefit of substantial savings in CPU time. The numerical solution of the EOS is based on Brent's method for the solution of nonlinear equations (Brent 1973) which is very robust and fast.

In addition to the non-LTE lines, the models include, self-consistently, line blanketing of the most important ($\approx 10^5$) metal lines selected from the latest atomic and ionic line list of Kurucz (1993). The entire list contains close to 4.2×10^6 lines, but not all of them are important for the case at hand. Therefore, before every temperature iteration, a shorter list is formed from the original list. First, an optical depth point is chosen, usually at $\tau_{\rm std} \approx 0.01$. Then, using the density and temperature for this depth the absorption coefficient in the line center, κ_l, is calculated for every line and compared to the corresponding continuum (LTE + non-LTE) absorption coefficient, κ_c. A line is transferred to the short list if the ratio $\Gamma \equiv \kappa_l/\kappa_c$ is larger than a prespecified value (usually 10^{-4}). In the subsequent radiative transfer calculations, all lines selected in this way are taken into account as individual lines, and all others from the large line list are neglected. This selection procedure is repeated at *every* iteration in order to always include the most important lines. We treat line scattering in the metal lines by parameterizing the albedo for single scattering, α. The calculation of α would require a full non-LTE treatment of *all* lines and continua, which is outside of the scope of this paper. Tests have shown that as a direct result of the velocity gradient in nova and supernova photospheres, the shape of the lines does not depend sensitively on α, and our approach is a reasonable first approximation (Hauschildt 1991; Nugent et al. 1995). Therefore, we adopt a constant value of $\alpha = 0.95$ for all metal lines, i.e., lines for which the level populations are treated in LTE. The continuous absorption and scattering coefficients are calculated using the cross sections as described in Hauschildt et al. (1992). In a typical run about 200,000 metal lines are treated in LTE, and 3300 lines are treated in non-LTE.

The effects of nonthermal collisional ionization by primary electrons produced by collisions with gamma rays due to the decay of ^{56}Ni and ^{56}Co are modeled using the continuous slowing down approximation (Garvey & Green 1976; Swartz 1991). We neglect the effect of secondary electrons, since most of their energy is themalized and thus does not affect the level populations directly (Meyerott 1980). The collisional cross sections are taken from the work of Lotz (1967a, b; 1968a, b, c).

2.2. *The Model Parameters*

The model atmospheres are characterized by the following parameters (see Hauschildt et al. 1992 for details):

1. The reference radius R_0, which is the radius where the continuum optical depth in extinction at 5000 Å is unity.
2. The effective temperature $T_{\rm eff}$, which is defined by means of the luminosity, L, and the reference radius, R_0 [$T_{\rm eff} = (L/4\pi R_0^2 \sigma)^{1/4}$ where σ is Stefan's constant].
3. The density structure parameter, v_e, [$\rho(r) \propto \exp(-v/v_e)$].
4. The expansion velocity, v_0, at the reference radius.
5. The density, $\rho_{\rm out}$, at the outer edge of the envelope.
6. The metal line threshold ratio, Γ.
7. The albedo for line scattering (metal lines only, here set to 0.95).
8. The statistical velocity ξ, treated as depth-independent isotropic turbulence.
9. The element abundances.

The influence of the nonthermal radiative and collisional excitation and ionization is discussed in detail in the subsequent sections.

We emphasize that for extended model atmospheres one should not assign, a priori, a physical interpretation to the parameter combination of $T_{\rm eff}$ and R_0. While $T_{\rm eff}$ has a well-defined physical meaning for plane-parallel stellar atmospheres, its definition for extended atmospheres is connected to the particular definition of the radius R_0 (see Baschek, Scholz, & Wehrse 1991). In addition, the reference radius R_0 in our models is defined using a *continuum* optical depth scale at $\lambda = 5000$ Å and is not directly comparable to observationally derived radii. Therefore, the effective temperature is not well defined for extended atmospheres and must be regarded only as a convenient numerical parameter.

We take the explosion date to be March 27–28 in order to scale the radii of our models (in § 9 we derive an explosion date of March 28.5 ± 1 day by minimizing the scatter in the distance estimates). We assume that the extinction to the supernova is given by $E(B-V) = 0.1$ mag (Baron et al. 1993; Jeffery et al. 1993; Wheeler & Filippenko 1994). In order to avoid calculational difficulties, we have treated Mg II and He II in LTE. The parameters for the models considered are given in Table 1. All of the model spectra are available electronically by request.

3. DISTANCE ESTIMATES

In our previous work (Baron et al. 1993; Baron et al. 1994) we have published distance estimates based on fits to spectra

TABLE 1

PARAMETERS OF THE MODELS PRESENTED IN THE FIGURES

Model	Spectrum	[He/H]	$T_{\rm eff}$	R_0 (10^{15} cm)	v_0 (km s^{-1})	v_e (km s^{-1})	N	$v_{\rm max}$ (km s^{-1})	$X_{\rm Ni}$
mar30_a.....	Mar 30	Solar	15000	0.2	...	...	50	15000	0.0
mar30_b.....	Mar 30	Solar	14000	0.3	20000	...	13	...	0.0
mar31_a.....	Mar 31	Solar	13000	0.3	...	...	50	15000	0.0
mar31_b.....	Mar 31	Solar	12000	0.75	...	...	50	38000	0.0
apr07_a	Apr 7	Solar	6500	1.0	12000	1000	...	...	0.03
apr07_b	Apr 7	2.01	6500	1.0	12000	800	...	...	0.03
apr07_c.....	Apr 7	2.01	6500	1.0	12000	1000	...	...	0.03
apr07_d	Apr 7	1.01	6500	1.0	12000	1000	...	...	0.03
apr07_e.....	Apr 7	0.01	6500	1.0	12000	1000	...	...	0.03
apr13_a	Apr 13	1.01	6000	1.3	9000	600	...	...	0.03
apr13_b	Apr 13	Solar	6000	1.3	9000	450	...	...	0.00
apr15_a	Apr 15	0.01	5900	1.4	9000	600	...	...	0.03
jun13_a.....	Jun 13	2.01	4500	6.0	7000	160	...	...	0.20
jun13_b	Jun 13	3.01	5000	6.0	7000	700	...	...	0.20
jun13_c.....	Jun 13	6.01	3000	6.0	5000	430	...	...	0.20

NOTE.—[He/H] is the logarithm of the ratio of the helium abundance to the hydrogen abundance (by number), but not normalized to the solar value ($= -1.01$), which we denote by "Solar." $T_{\rm eff}$, R_0, and v_0 are the "effective" temperature, radius, and velocity at the reference point $\tau_{\rm std} = 1$; v_e is the parameter that characterizes the exponential density profiles; N is the power-law density index; $v_{\rm max}$ is the maximum velocity (one can choose to specify either v_0 or $v_{\rm max}$); and $X_{\rm Ni}$ is a parameter that specifies the mass fraction of nickel to take into account the effects of nonthermal ionization.

obtained on April 7, April 13, and April 15. Since our models predict the absolute flux, we can use our spectra to calculate synthetic photometry given a set of filter responses and calibration. In our previous work we had used and B and V filters of Azusienis & Straizys (1969) using the blackbody calibration of Schurmann (1983). In this paper we have used the *UBVRI* filters of Bessell (1990). Sixteen Baldwin-Stone photometic standard stars were measured by Landolt (1992), and these measurements were used along with spectrophotometry from Hamuy et al. (1992) in order to perform the calibration. We note that our new absolute magnitudes, which should be far more accurate than our previous values, are also about 0.5 mag brighter than our previous values in both B and V. For the two epochs for which we have flux-calibrated spectra (April 7 and April 15), synthetic photometry agrees with observational photometry to ± 0.1 mag.

Our results are listed in Table 2. We have derived the distances by subtracting our calculated absolute magnitudes from the published photometry (Richmond et al. 1994) and assuming an extinction of $A_V = 0.31$ mag and $A_B = 0.41$ mag. We shall discuss the distance obtained from each observed spectrum in turn.

4. 1993 MARCH 30–31

The early spectra (Fig. 1) are remarkably featureless with weak Hα. The peaks and valleys between 5000 Å and 5800 Å in the March 30 Lick spectrum are probably due to calibration errors; however, the prominent features blueward of 5000 Å in the La Palma spectra are likely to be real (Lewis et al. 1994; R. Cumming 1994, private communication). Figures 2 and 3 show our model calculations mar30_a and mar31_a, our best fits to the data taken on March 30 and 31, respectively. For the March 31 observed spectrum we have used a composite of the spectra taken by Jim Liebert in the blue and by Peter Garnavich and Hong Bae Ann in the red (see Fig. 1). While the

TABLE 2

ABSOLUTE MAGNITUDES AND DISTANCE ESTIMATES

Model	Spectrum	M_B	M_V	$(B-V)$	μ_B	μ_V	ζ_B
mar30_a.....	Mar 30	−15.67	−15.57	−0.09	26.03	25.78	0.60
mar30_b.....	Mar 30	−15.59	−15.40	−0.18	25.95	25.61	0.42
mar31_a.....	Mar 31	−16.20	−16.15	−0.05	26.85	26.47	0.59
mar31_b.....	Mar 31	−18.08	−18.05	−0.03	28.73	28.68	0.59
apr07_a	Apr 7	−16.83	−17.04	0.20	28.61	28.46	0.49
apr07_b	Apr 7	−17.01	−17.32	0.32	28.79	28.74	0.73
apr07_c.....	Apr 7	−17.01	−17.33	0.32	28.79	28.75	0.74
apr07_d	Apr 7	−16.93	−17.32	0.39	28.71	28.74	0.85
apr07_e.....	Apr 7	−16.86	−17.12	0.27	28.64	28.54	0.59
apr13_a	Apr 13	−16.92	−17.27	0.35	28.08	27.94	0.63
apr13_b	Apr 13	−16.87	−17.20	0.33	28.03	27.87	0.57
apr15_a	Apr 15	−17.02	−17.40	0.38	28.04	27.91	0.62
jun13_a.....	Jun 13	−17.44	−18.84	1.40	30.98	31.47	3.2
jun13_b	Jun 13	−16.94	−18.34	1.40	30.48	30.97	2.6
jun13_c.....	Jun 13	−18.13	−18.63	0.50	31.67	31.26	0.59

NOTE.—The table lists the absolute magnitudes and $(B-V)$ colors. The absolute magnitudes and distance moduli have all been adjusted so that the radii models all correspond to an explosion date of March 28.0. In calculating the distance moduli we have assumed extinction $A_V = 0.31$ mag and $A_B = 0.41$ mag. Also listed is the dilution factor ζ_B.

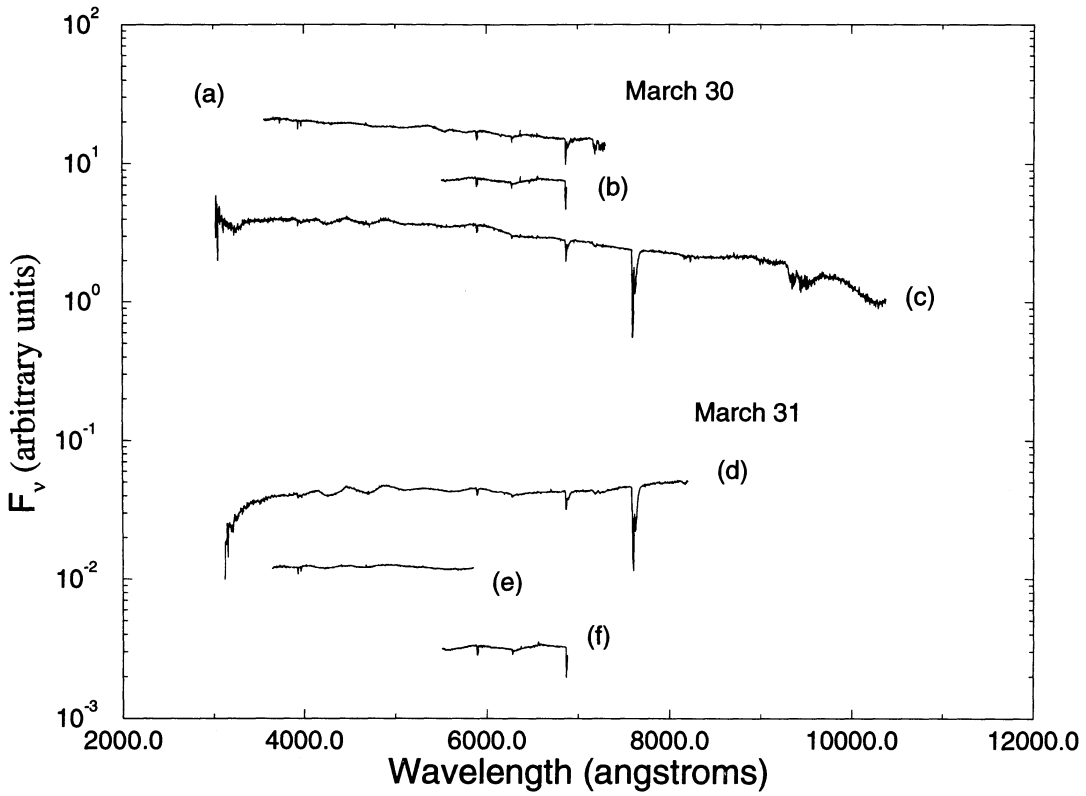

FIG. 1.—March 30 and March 31 data compared. Spectrum (a) was taken at Lick Observatory (Filippenko et al. 1993) on March 30.2 UT; spectra (b) and (f) were taken by Peter Garnavich and Hong Bae Ann on March 30.4 UT and March 31.5 UT, respectively; spectra (c) and (d) were taken at La Palma (Lewis et al. 1994) on March 30.9 UT and April 1.05, respectively; and spectrum (e) was taken by Jim Liebert on March 31.2 UT. The absorption features at 6860 Å, 7200 Å, 7600 Å, and 9400 Å are telluric.

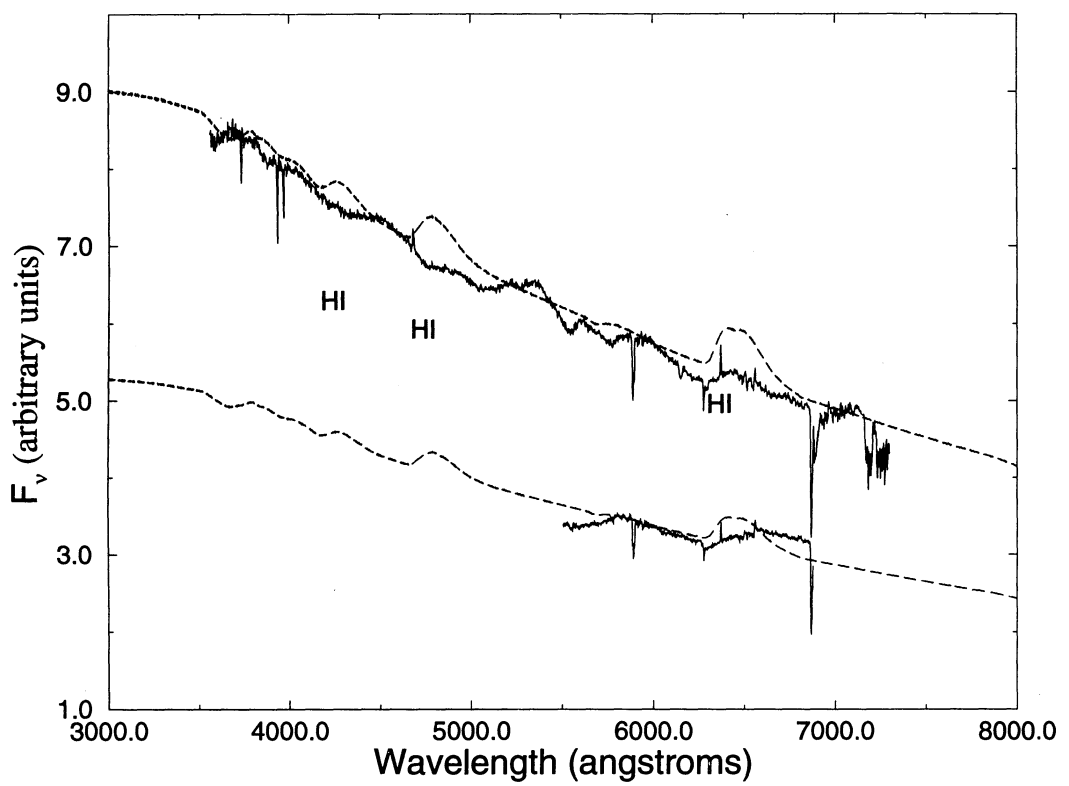

FIG. 2.—March 30, Model mar30_a is compared to the observed spectrum taken at Lick Observatory (Filippenko et al. 1993; *upper curve*) and by Peter Garnavich and Hong Bae Ann (*lower curve*). The features between 5000 Å and 5800 Å in the Lick spectrum are probably due to calibration errors. The absorption feature at 6860 Å and 7200 Å are telluric, as is the weak narrow line at 6280 Å.

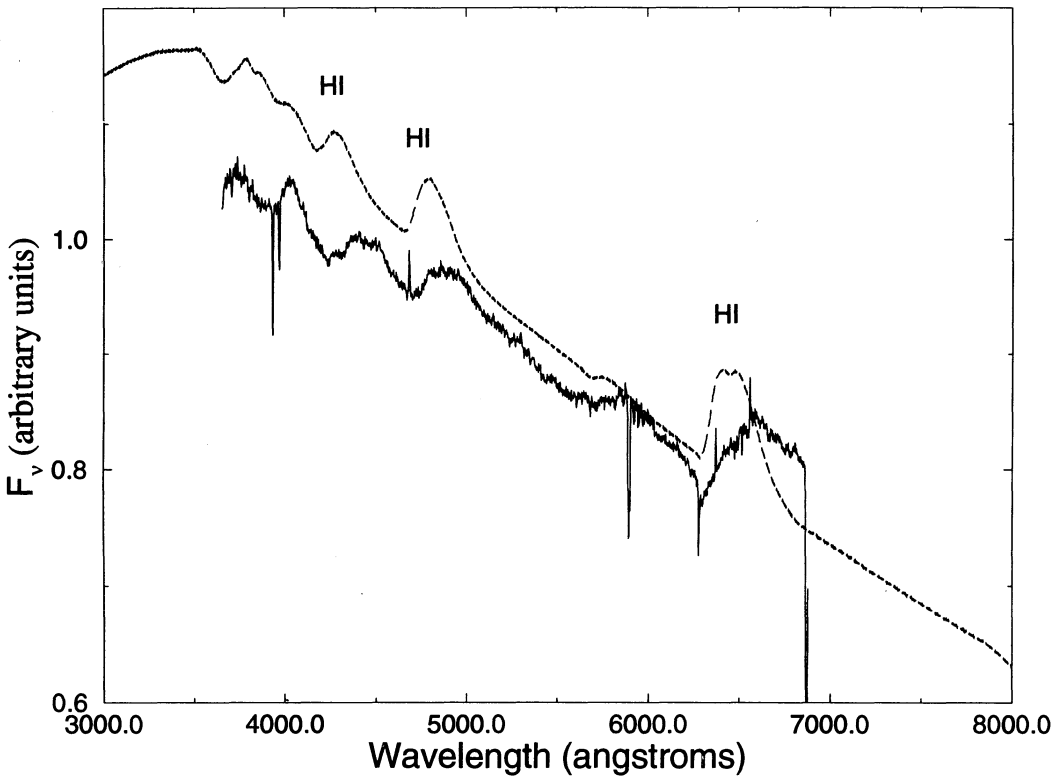

FIG. 3.—March 31, Model mar31_a is compared to the observed spectrum, where the observed spectrum is a composite of the blue spectrum obtained by Jim Liebert and the red spectrum obtained by Peter Garnavich and Hong Bae Ann. The narrow absorption features at 6280 Å and 6860 Å are telluric.

continuum is well fitted, the computed Hα is too strong and too wide in emission. In these fits the density profile is essentially that of a "brick wall" with a power-law index $N = 50$ and the maximum velocity $v_{max} = 15{,}000$ km s^{-1}. We also obtain reasonably good fits with $N = 13$ and the photospheric velocity $v_0 = 20{,}000$ km s^{-1} (model mar30_b), but the fit is not as good, since the Balmer lines are stronger in the extended model than in the brick wall model. The actual value of the density exponent is not well determined by our models, since none of the models fit the lineshapes well, but it is likely that its value is high.

Freedman et al. (1994) have measured the Cepheid distance to M81, the parent galaxy of SN 1993J, as $\mu = 27.8 \pm 0.2$ mag. Our estimates for the March spectra (Table 2) are far too low, leading us to question the validity of the fits.

It is worthwhile to review the assumptions we employ to estimate the distance to the supernova:

1. Homologous expansion $v \propto r$, from which it follows that the velocity of a given matter element is constant and hence the position of our reference radius is just given by $v_0 t$, where t is measured from the time of explosion.
2. The density follows a power law or decaying exponential.
3. Our solutions of the radiative transport equations are correct.
4. A high-quality fit to the spectrum implies that we accurately determined the model parameters.

The assumption of homology may be suspect at these early times. In order to increase the brightness of the models by 2 mag, assuming that we have fitted the underlying continuum correctly, we require an error in the reference velocity of a factor of 2.5. Since the usual velocity diagnostics of line shapes are not available here, this is not improbable. Figure 4 shows the synthetic spectrum for model mar31_b, which has higher velocities than model mar31_a. While Hα is too blueshifted, the overall continuum and the other features are not fit discernibly more poorly than in our other calculations. In addition, if there were significant deceleration of the ejecta at early times, we could get large radii with smaller velocities, giving better fits to the line shapes.

It is difficult to understand what physical mechanism could produce an atmosphere as steep as $N = 50$. If the initial (preshocked) atmosphere were very steep, the shock wave accelerating down the density gradient would produce a flatter postshocked atmosphere. The ram pressure due to the shock is so strong that it is implausible any kind of circumstellar interaction could have led to such a steep density profile. On the other hand, no model we have considered, steep or flat, gives both a reasonable distance and a reasonable velocity. The early time atmosphere of SN 1993J is not well understood.

5. 1993 APRIL 7

This is the first optical spectrum we have computed that shows clear evidence of helium with a strong He I λ5876 line and a clear notch in the Hα emission peak which is tempting to identify as being due to He I λ6678. A good fit is obtained by models having a very steep density profile with an effective power-law index at the reference radius $N = 23$ (Baron et al. 1993). The synthetic spectrum shows evidence of unblended features near 4000 Å which are also present in the observed spectrum; however the Balmer lines and He I lines are far too narrow. The best fit to the Hα emission profile is shown in Figure 5 (model apr07_e), which has a much shallower density profile, $N = 12$ at the reference radius. In both models the

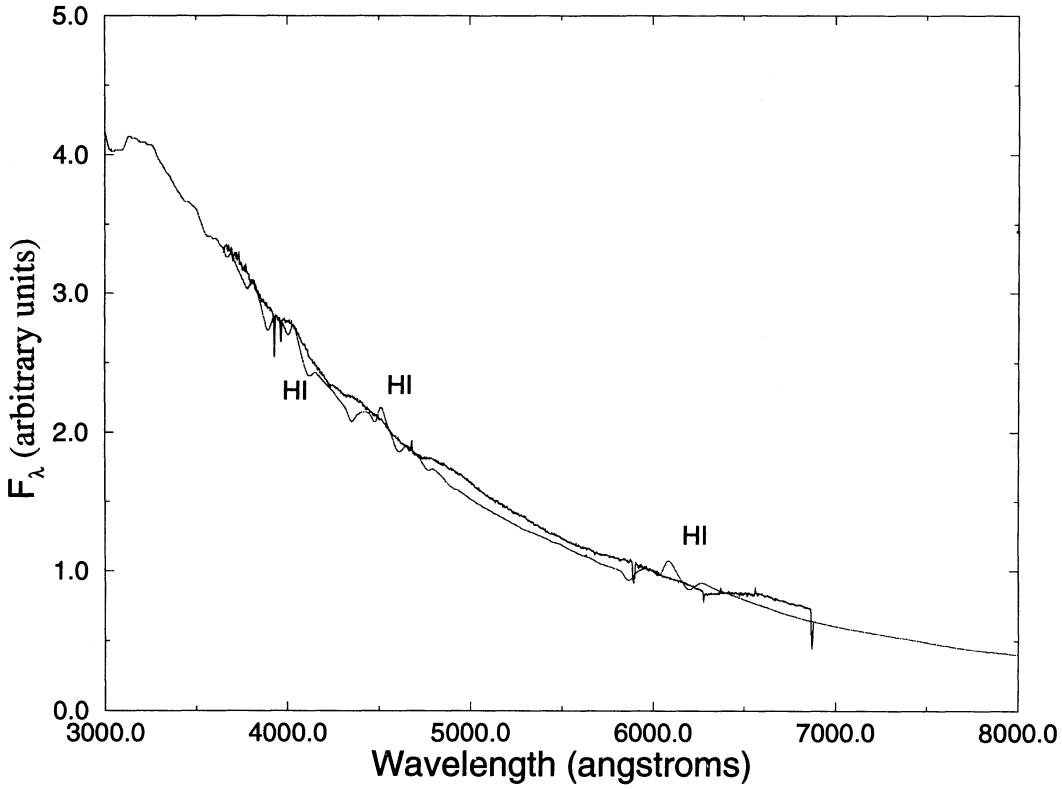

FIG. 4.—March 31, Model mar31_b is compared to the composite observed spectrum. The ordinate in this and subsequent figures is F_λ as opposed to F_ν.

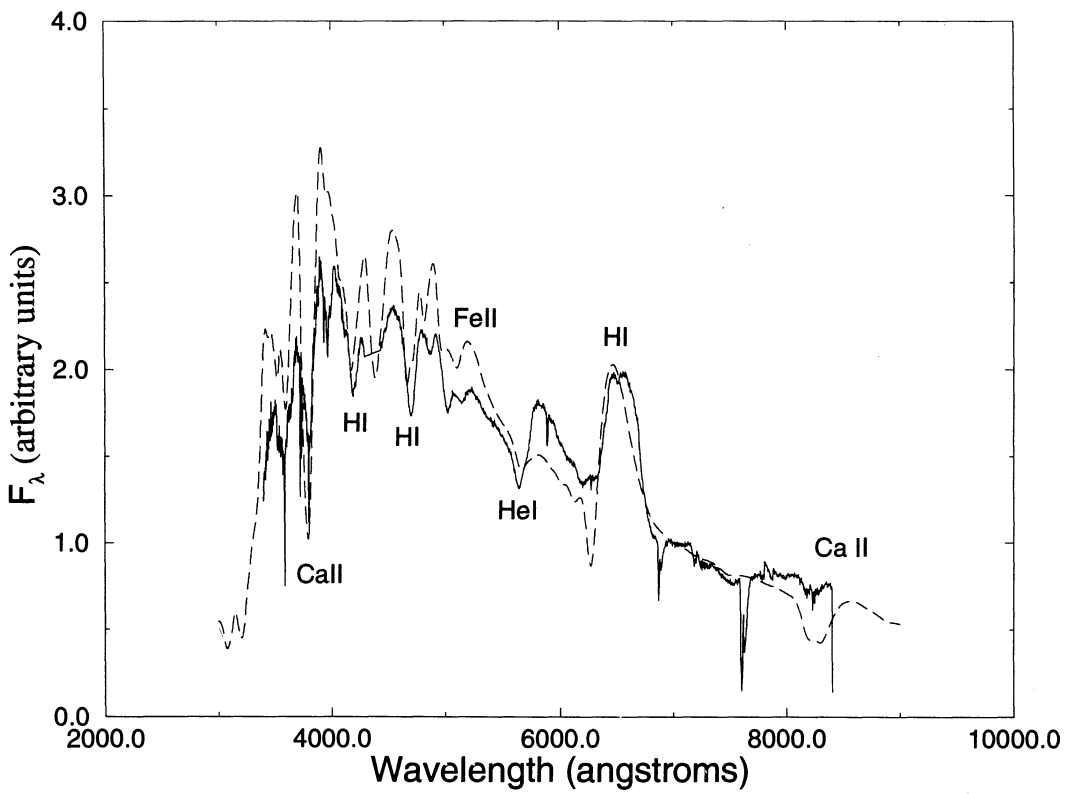

FIG. 5.—April 7, Model apr07_e is compared to the observed spectrum taken at Lowell Observatory by Mark Wagner and Scott Austin (Baron et al. 1993)

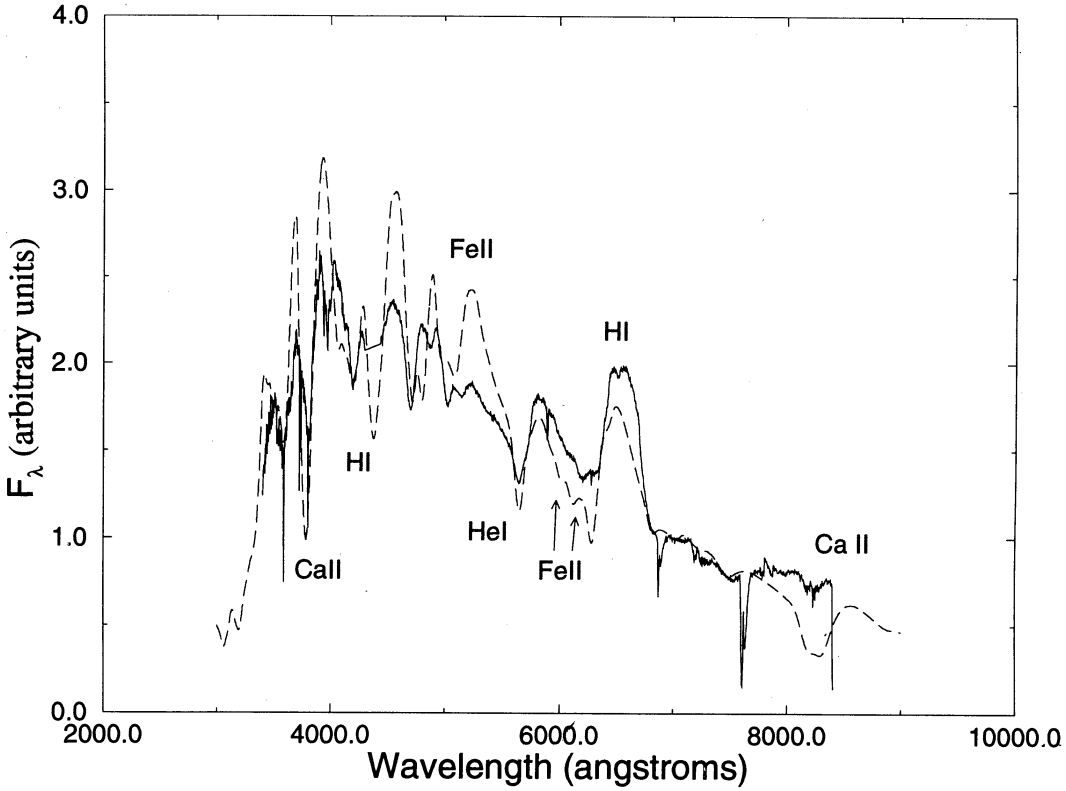

FIG. 6.—April 7, Model apr07_d is compared to the observed spectrum taken at Lowell Observatory by Mark Wagner and Scott Austin (Baron et al. 1993)

hydrogen to helium ratio is equal by number ($Y = 0.8$), and the emission and absorption of the He I λ5876 line is too weak. In addition, the observed notch in the top of the Hα profile, if real, can only be produced by the He I λ6678 line. Figure 6 shows model apr07_d, where the helium is enhanced by a factor of 10 over hydrogen by number. This model gives a reasonable fit to the He I λ5876 line and even shows some evidence of an asymmetry in the Hα emission. Further enhancing helium, to 100 times hydrogen (see model apr07_c), does a much better job of fitting the He I λ5876 line, particularly in emission, but the Hα emission is now far too weak; however, the "notch" due to He I λ6678 is in the right place, with roughly the right strength. It is likely that the observed spectrum is due to a nonuniform composition, with the photosphere having receded into the helium layer of the star and the Hα emission being formed by a shell of hydrogen-rich material farther out. Hydrogen cannot be entirely absent from the photospheric region since the weaker Balmer lines form in this region and are well fitted by model apr07_d and not as well fitted by model apr07_c.

Another problem with the models is that none of them fit the extended absorption blueward of Hα, even though the emission profile is well fitted. Although we have previously suggested (Baron et al. 1993; Baron et al. 1994) that this may be due to a layer of hydrogen at high velocity, Figure 6 shows that the absorption is likely due to strong Fe II features such as λ6247, λ6148 and λ6084 blended with other Fe II features. Non-LTE effects probably cause the poor fit to these lines.

6. 1993 APRIL 13–15

At this time the photospheric velocity has dropped to about $v_0 = 9000$–$11{,}000$ km s^{-1}, and the photospheric temperature has dropped to about $T_0 = 6000$ K. Figure 7 shows the fit for model apr13_b, with $v_0 = 9000$ km s^{-1}, $R_0 = 1.3 \times 10^{15}$ cm, $T_0 = 6000$ K, and $v_e = 450$ km s^{-1}, with a solar ratio of hydrogen to helium and no nonthermal ionization. Figure 8 displays a similar model (apr13_a) where v_e has been increased to 600 km s^{-1}, but now helium has been enhanced to $Y = 0.8$, and nonthermal ionization is included. Model apr13_a does much better at fitting the profiles of both Hα and He I λ5876 due to the inclusion of nonthermal ionization; the blue is better fitted in model apr13_b with the steeper density profile. As is the case for the April 7 models, the poor fit of the extended blueward absorption of Hα is likely due to NLTE effects in Fe II. The computed absorption of the Hα feature is too deep which is probably due to the fact that the emission from the Fe II features is too weak in our models, and so some of the absorption in Hα is reduced by blending with Fe II emission. Such blending makes empirical estimates of the blueward extent of the Hα feature rather difficult.

On April 15, there is both a *HST* UV and an optical spectrum (Jeffery et al. 1993). We have previously (Baron et al. 1994) found the best-fit parameters to be (model apr15_a) $v_0 = 9000$ km s^{-1}, $R_0 = 1.4 \times 10^{15}$ cm, $T_0 = 5900$ K, and $v_e = 600$ km s^{-1}. The spectrum is displayed in Figure 9. This model also has enhanced helium, $Y = 0.8$, and nonthermal ionization corresponding to a nickel mass fraction $X_{\rm Ni} = 0.03$ was included. The photospheric velocity remains constant over the 2 days, but the higher e-folding velocity ($v_e = 600$ km s^{-1}) is now clearly preferred, perhaps indicating that the atmosphere is getting flatter.

One of the most interesting differences between the observed and theoretical spectra is in the UV below $\approx$3000 Å. The

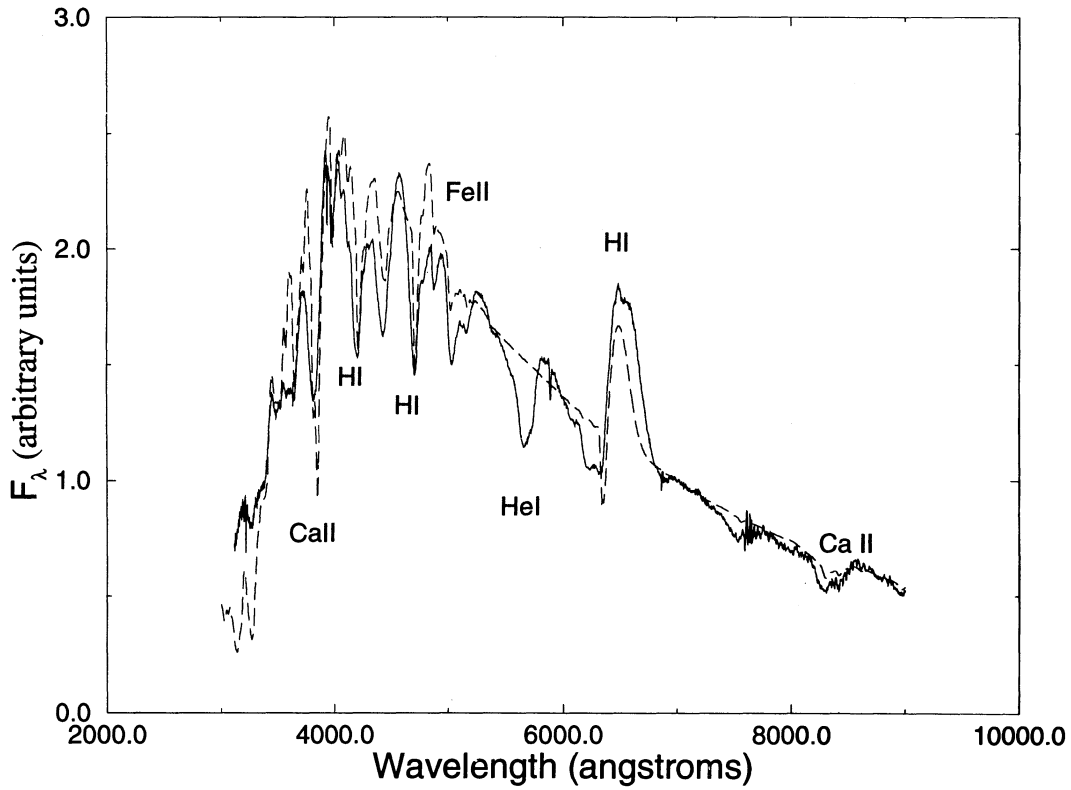

FIG. 7.—April 13, Model apr13_b is compared to the observed spectrum taken at Lick Observatory by Alex Filippenko and Tom Matheson (Baron et al. 1993)

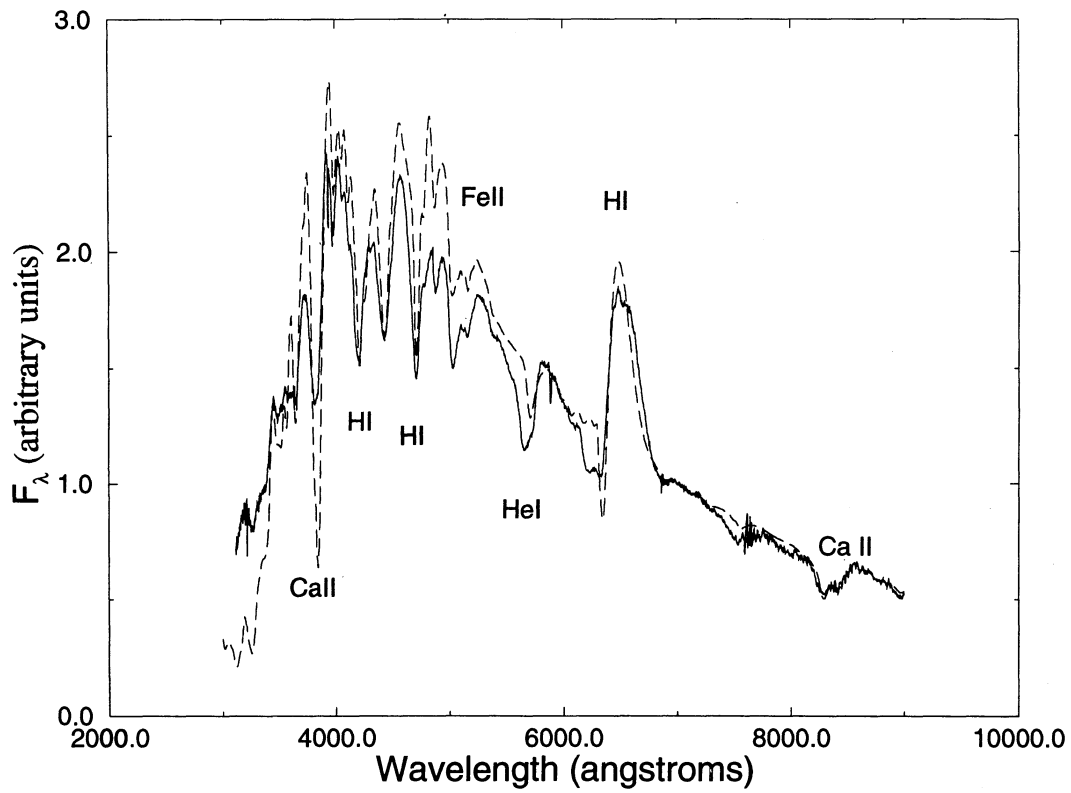

FIG. 8.—April 13, Model apr13_a is compared to the observed spectrum taken at Lick Observatory by Alex Filippenko and Tom Matheson (Baron et al. 1993)

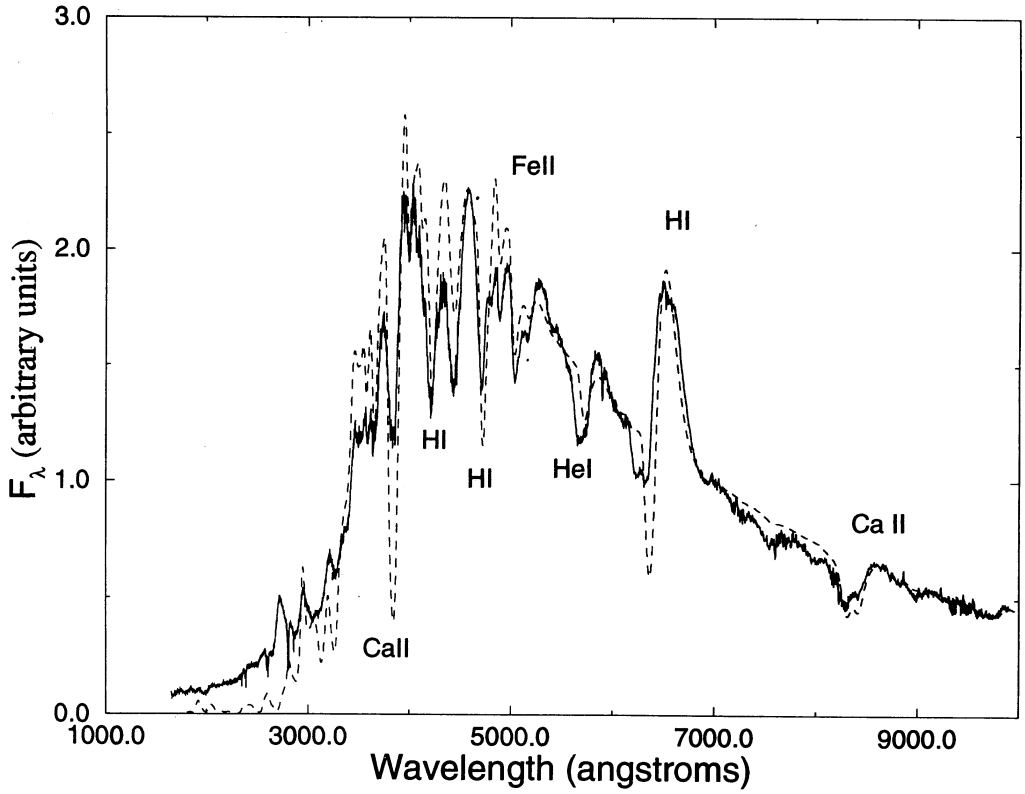

FIG. 9.—April 15, Model apr15_a is compared to the observed spectrum taken by the HST and at Lick Observatory (Jeffery et al. 1993)

theoretical spectrum drops off very rapidly in the UV, whereas the observed spectrum is nearly flat. This occurs in all of our models that provide reasonable fits to the red. The ratio of the observed flux $F_{obs}(2000)/F_{obs}(1750) \approx 1$. It is very difficult to understand how to get this much UV flux out of the supernova. Let us denote the observed flux by $F_{obs}(\lambda)$, the computed flux by $F(\lambda)$, and the flux of a blackbody with the same effective temperature as our computed flux as $\pi B(\lambda)$. If we compare our computed spectrum to that of a blackbody, i.e., we neglect the effects of line blanketing in the UV, then we find the ratio $\pi B(\lambda)/F(\lambda) = 8$ (66) at $\lambda = 2000$ (1750) Å, whereas the ratio of the observed to the computed flux $F_{obs}(\lambda)/F(\lambda) = 9$ (222) at $\lambda = 2000$ (1750) Å. Thus, since $\pi B(1750)/\pi B(2000) = 0.59$, even if the supernova were totally transparent in the UV down to the photosphere, there would not be enough flux to reproduce the observations. Of course, the effects of line blanketing cause the supernova to be strongly absorbing in the UV. With either a Planckian or thermal bremsstrahlung spectrum, it is difficult to understand the relative flux remaining nearly constant, since for a Planckian spectrum the ratio of the flux should go as $(\lambda_1/\lambda_2)^4$, whereas for a thermal bremsstrahlung spectrum the ratio scales somewhat more slowly, $(\lambda_1/\lambda_2)^2$. Thus, neither a clumping of the ejecta with small filling factor, nor external emission caused by a circumstellar interaction, seems to explain the observations adequately. In addition, it is very difficult to understand how to get such large UV fluxes out of a circumstellar interaction, given that the total X-ray luminosity was $\lesssim 10^{40}$ ergs s^{-1}.

7. 1993 JUNE 13

By June 13, the spectrum has become more complicated. The supernova is making the transition to a nebular spectrum although there is still a well-developed continuum. The Hα line now exhibits clear "double-peaked" structure, likely due to He I λ6678. The photosphere has receded into the helium shell, but the Balmer lines are forming in a thin shell of material above the photosphere. This complicated structure taxes our modeling ability with our current assumption of uniform compositions. Figure 10 displays model jun13_a with [He/H] = 2,[8] which does a reasonable job of fitting the Balmer lines, but there is no evidence of a double-peaked structure in Hα and the He I λ5876 line is not strong enough. Increasing [He/H] to 3 (Fig. 11; model jun13_b) produces a more pleasing fit, and does quantitatively better on the He I λ5876 feature, but the double peak still remains elusive. Figure 12 displays model jun13_c where [He/H] = 6, i.e., hydrogen has been reduced to a trace. Now there is evidence of the He I λ6678 feature, but Hα is not strong enough. This spectrum appears very blue, due to a decrease of line blanketing in the U band; as the number of lines decreases the flux generally passed to the red is allowed to escape, making the spectrum look blue even though it is very cold. It goes without saying that more work remains to be done in order to fit this epoch. Models with nonuniform composition are certainly required. Since the photosphere will have long receded into the helium shell, this is not unexpected. While it is not possible to draw quantitative conclusions from our models, it seems likely that there was little if any mixing of the hydrogen shell into the helium layers, in contrast to SN 1987A. The density profile has significantly flattened with power-law indices $N \approx 7$–12 being appropriate at this time, but the hydrogen shell requires steeper profiles to reproduce

[8] We use the notation [He/H] = $\log_{10}(n_{He}/n_H)$, and we do not use the standard convention of normalizing to the solar value.

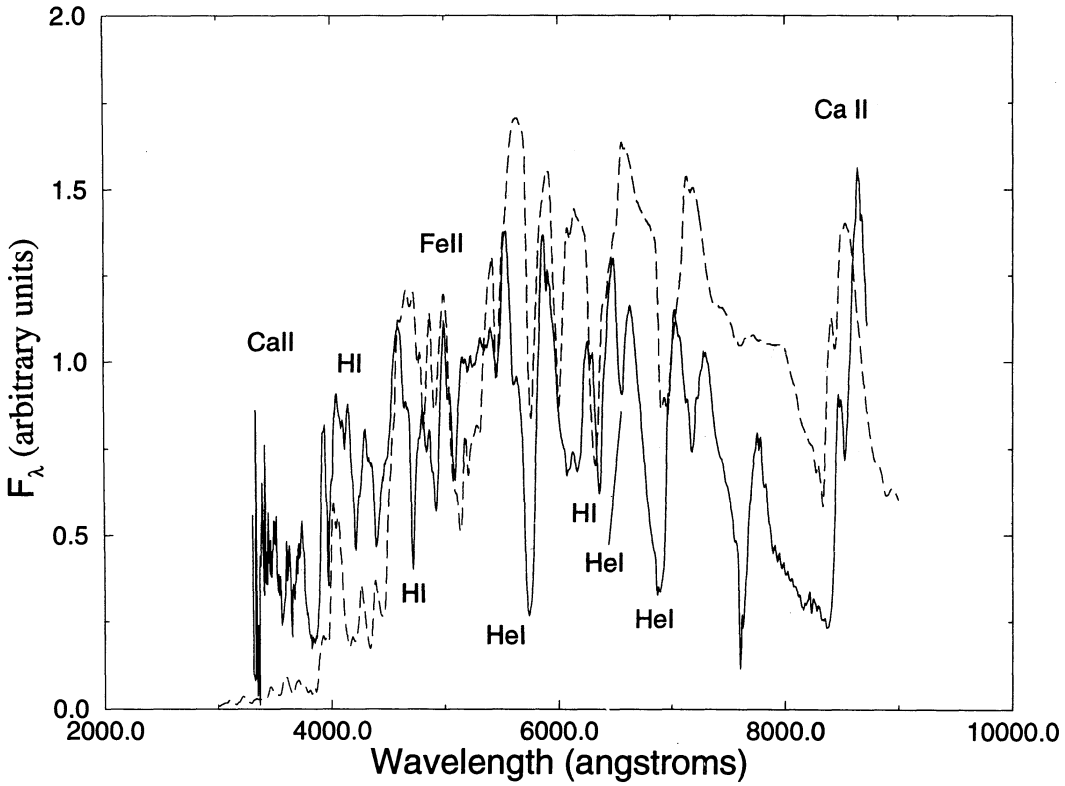

FIG. 10.—June 13, Model jun13_a is compared to the observed spectrum taken by Scott Austin and Mark Wagner

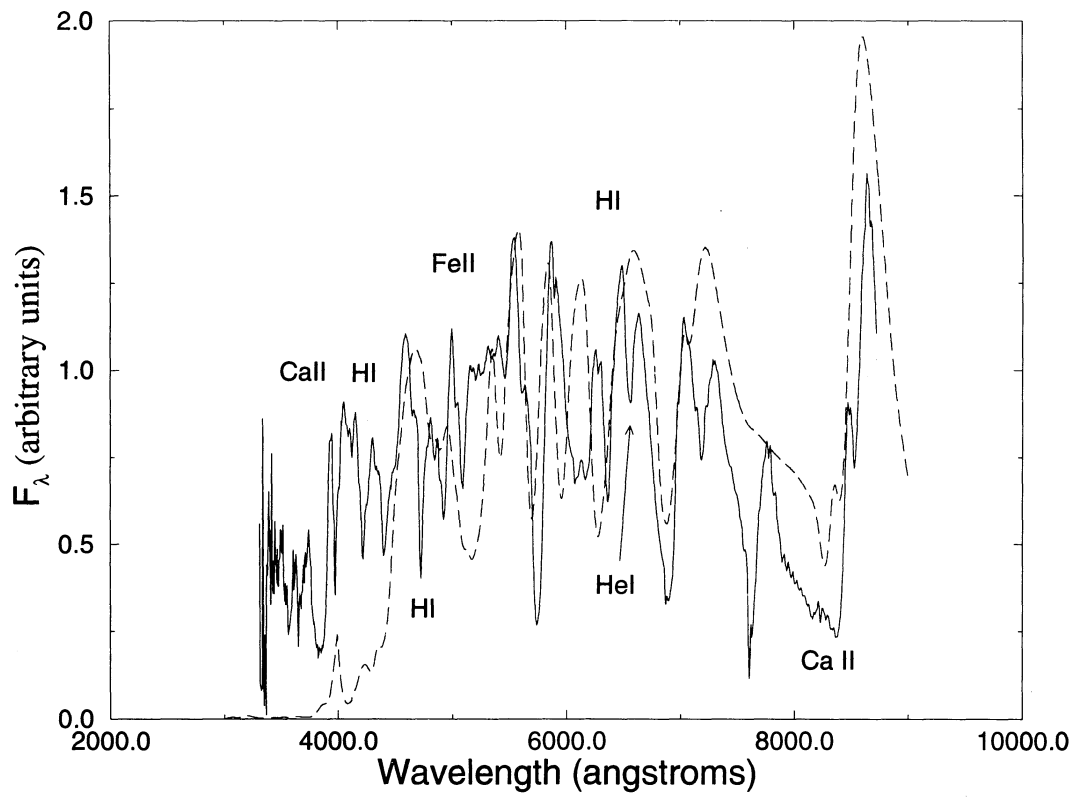

FIG. 11.—June 13, Model jun13_b is compared to the observed spectrum taken by Scott Austin and Mark Wagner

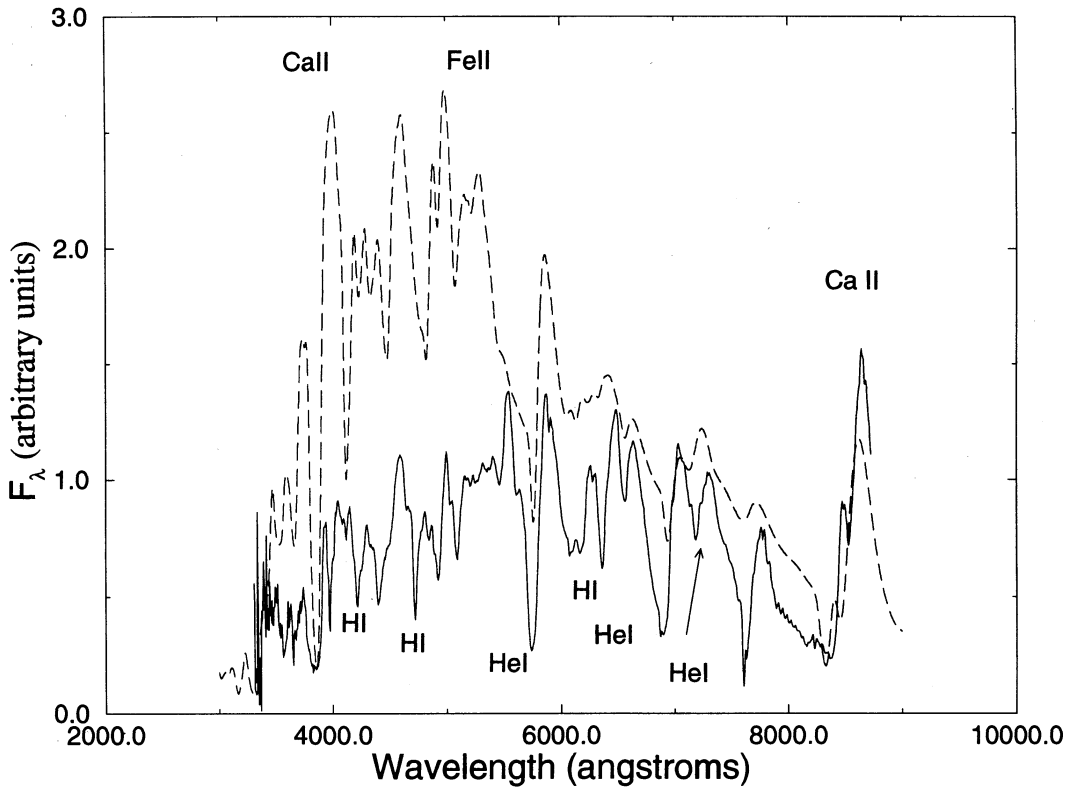

FIG. 12.—June 13, Model jun13_c is compared to the observed spectrum taken by Scott Austin and Mark Wagner

the narrow lines. It is easy to dismiss the outrageously large distance estimates from the June 13 epoch, since the quality of the fits is so low.

8. DISCUSSION

Clearly, there is a large drift in the mean apparent distance from epoch to epoch (Table 2). If we use only the results of our fits for the month of April then our distance estimate is $\mu = 28.2 \pm 0.4$ mag, within the uncertainties of both the Cepheid measurement ($\mu = 27.8 \pm 0.2$ mag; Freedman et al. 1994) and our previous distance measurements (Baron et al. 1993; Baron et al. 1994). It seems not unreasonable to restrict ourselves to our best fits, since the April models are the only ones where we can truly claim to have fitted the entire spectrum and not just a portion (admittedly, the far UV is not well fit on April 15).

Since the application of the expanding photosphere method depends on the uncertain explosion date, one wishes to give lower weight to early spectra, since a longer time baseline minimizes the error due to uncertainties in the explosion date. The best fits to the observed spectra, with the longest time baseline, are for the epoch April 13–15, and that is where the distance is in closest agreement with the Cepheid value. In fact, confining ourselves to that epoch alone, our result is $\mu = 28.0 \pm 0.1$ mag, in excellent agreement with the Cepheid value. Using all the April data we obtain even closer agreement with the Cepheid value and reduce the scatter in the estimates by taking the explosion date to be March 29; in this case we obtain $\mu = 28.0 \pm 0.3$ mag. We thus conclude that the explosion date is March 28.5 ± 1 day.

Both polarization data (Trammell, Hines, & Wheeler 1993) and VLBI data (Marcaide et al. 1994) indicate significant asymmetry in the supernova, which our models do not address. The good fits and distance estimates in April may be a fortuitous coincidence, but if that were the case it would be remarkable.

9. DILUTION FACTORS

In comparing detailed calculations to simple analytic ones, it has been customary to introduce dilution factors, which relate the actual luminosity to that of some given black body. Hershkowitz, Linder, & Wagoner (1986) have discussed the dilution of the flux over that of a blackbody with the same color temperature due to the frequency dependence of the position of the photosphere in a scattering dominated atmosphere.

Schmidt, Kirshner, and Eastman (Schmidt, Kirshner, & Eastman 1992; Eastman & Kirshner 1989) have introduced an observationally defined dilution factor

$$\zeta_X^2 = \frac{\int S_X(\lambda) F_{\rm obs}(\lambda) d\lambda}{\int S_X(\lambda) \pi B_\lambda(T_{B-V}) d\lambda},$$

where the color temperature T_{B-V} is determined from the observational colors using the relation

$$T_{B-V} = \frac{10^4 \text{ K}}{1.605(B-V) + 0.67}.$$

$S_X(\lambda)$ is the filter response function for spectral band X, and we have chosen to use the B band. The value of ζ is reasonably constant over the bands BVR and very constant over BV.

A relationship between ζ and color temperature has been used by Schmidt et al. (1992, 1994a, b) to estimate the Hubble constant by means of a version of the expanding photosphere

method applied to Type II supernovae. Comparing the relation between ζ_B and color temperature for our models with the relations displayed by Schmidt (1993) we find good qualitative agreement, but our dilution factors suggest intrinsic scatter in the relation and tend to be greater than those of Schmidt (1993) by about 60%. To first order, then, if our models were used in the Schmidt et al. (1994b) version of the expanding photosphere method, they would produce distances that are larger by some 60% and reduce the estimated Hubble constant by the same amount.

10. CONCLUSIONS

We have calculated detailed synthetic spectra for comparison with spectra of SN 1993J obtained at the end of March, over the first 2 weeks of April, and in mid-June of 1993. Our fits for spectra obtained in April are quite good, with the best fits obtained for spectra in the epoch April 13–15. While we are able to reproduce the continuum of the March spectra quite well, all of our models produce strong, unseen Balmer lines. We are able to reduce the strength of the Balmer lines, as well as to obtain the best fit to the continuum, by using a very steep, "brick wall" atmosphere. With little extension, the Balmer emission is suppressed. The distance estimates obtained with these fits, however, call into question the accuracy of the model parameters.

All of our models for spectra obtained after March 31 show evidence for nonuniform compositions—that is, there is a clear separation between the hydrogen and helium layers, so there must have been little mixing of hydrogen to deeper layers, in contrast to the situation in SN 1987A. On the other hand, the strong helium lines can only be excited by gamma rays produced by nickel mixed into the helium layers at early times.

Our distance estimates show that accurate results can be obtained with the expanding photosphere method, but only if one confines the distance estimates to the best fits of the observed spectra. Obviously one must use synthetic spectra that provide good fits to the observed spectra in order to predict the emitted flux. Quantifying the quality of fit needed to extract distances remains the subject of future work.

We thank Robert Cumming, David Jeffery, Lisa Ensman, Brian Schmidt, Giora Shaviv, Sumner Starrfield, and Rainer Wehrse for helpful discussions; David Jeffery, the La Palma group, and the SINS team for providing spectra electronically in advance of publication; M. Davis and D. Schlegel for obtaining the March 30 Lick spectrum; and Thomas Vaughan for assistance in calibrating our synthetic photometry. The Isaac Newton Telescope is operated on the island of La Palma by the Royal Greenwich Observatory in the Spanish Observatorio del Roque de los Muchachos of the Instituto de Astrofisica de Canarias. This work was supported in part by NASA grant NAGW-2999; a NASA LTSA grant to ASU; NASA grant GO-2563.01-87A from the Space Telescope Science Institute, which is operated by the Association of Universities for Research in Astronomy, Inc.; and by NSF grants AST 91-15061 and AST 91-15174. Some of the calculations in this paper were performed at the NERSC, supported by the US DoE, and at the San Diego Supercomputer Center, supported by the NSF; we thank them for a generous allocation of computer time.

REFERENCES

Aldering, G., Humphreys, R. M., & Richmond, M. 1994, AJ, 107, 662
Allard, F., Hauschildt, P. H., Miller, S., & Tennyson, J. 1994, ApJ, 426, L39
Azusienis, A., & Straizys, V. 1969, Soviet Astr.-AJ, 13, 316
Baade, W. 1926, Astr. Nach., 228, 359
Baron, E., Hauschildt, P. H., & Branch, D. 1994, ApJ, 426, 334
Baron, E., Hauschildt, P. H., Branch, D., Wagner, R. M., Austin, S. J., Filippenko, A. V., & Matheson, T. 1993, ApJ, 416, L21
Bartunov, O. S., Blinnikov, S. I., Pavlyuk, N. N., & Tsvetkov, D. 1994, A&A 281, L53
Baschek, B., Scholz, M., & Wehrse, R. 1991, A&A 299, 374
Bessell, M. S. 1990, PASP, 102, 1181
Branch, D., Falk, S. W., McCall, M. L., Rybski, P., Uomoto, A. K., & Wills, B. J. 1981, ApJ, 244, 780
Brent, R. P. 1973, Algorithms for Minimization without Derivatives (Englewood Cliffs, NJ: Prentice-Hall)
Chevalier, R. A. 1984, Ann. NY Acad. Sci., 422, 215
Eastman, R., & Kirshner, R. P. 1989, ApJ, 347, 771
Filippenko, A. V., & Matheson, T. 1993, IAU Circ., No. 5787
Filippenko, A. V., Matheson, T., & Ho, L. C. 1993, ApJ, 415, L103
Fransson, C., Lundqvist, P., & Chevalier, R. 1994, ApJ, submitted
Freedman, W. L., et al. 1994, ApJ, 427, 628
Garvey, R. H., & Green, A. E. S. 1976, Phys. Rev. A, 14, 946
Hamuy, M., Walker, A. R., Stuntzeff, N. B., Gigoux, P., Heathcote, S. R., & Phillips, M. M. 1992, PASP, 104, 533
Hauschildt, P. H. 1991, Ph.D. thesis, Universität Heidelberg
———. 1992a, J. Quant. Spectrosc. Rad. Transf., 47, 433
———. 1992b, ApJ, 398, 224
———. 1993, J. Quant. Spectrosc. Rad. Transf., 50, 301
Hauschildt, P. H., Best, M., & Wehrse, R. 1991, A&A, 247, L21
Hauschildt, P. H., Starrfield, S., Austin, S., Wagner, R. M., Shore, S. N., & Sonneborn, G. 1994, ApJ, 422, 831
Hauschildt, P. H., Wehrse, R., Starrfield, S., & Shaviv, G. 1992, ApJ, 393, 307
Hershkowitz, S., Linder, E., & Wagoner, R. 1986, ApJ, 303, 800
Höflich, P., Langer, N., & Duschinger, M. 1993, A&A, 275, L29
Hu, J. Y., Li, Z. W., Jiang, X. J., & Wang, L. F. 1993, IAU Circ., No. 5777
Jeffery, D. J., et al. 1993, ApJ, 421, L27
Kirschner, R. P., & Kwan, J. 1974, ApJ, 193, 27
Kurucz, R. 1993, CD-ROM No. 1, Atomic Data for Opacity Calculations, Smithsonian Astrophysical Observatory, Cambridge, MA
Landolt, A. U. 1992, AJ, 104, 372
Leising, M., et al. 1994, ApJ, 431, L95
Lewis, J. R., et al. 1994, MNRAS, 266, L27
Lotz, W. 1967a, ApJS, 14, 207
———. 1967b, J. Opt. Soc. Am., 57, 873
———. 1968a, J. Opt. Soc. Am., 58, 236
———. 1968b, J. Opt. Soc. Am., 58, 915
———. 1986c, Z. Phys., 216, 241
Marcaide, J., et al. 1994, BAAS, in press
Meyerott, R. E. 1980, ApJ, 239, 257
Nomoto, K., Suzuki, T., Shigeyama, T., Kumagai, S., Yamaoka, H., & Saio, H. 1993, Nature, 364, 507
Nugent, P., Baron, E., Hauschildt, P. H., & Branch, D. 1995, ApJ, submitted
Podsiadlowski, P., Hsu, J. J. L., Joss, P. C., & Ross, R. R. 1993, Nature, 364, 509
Podsiadlowski, P., Joss, P. C., & Hsu, J. J. L. 1992, ApJ, 391, 245
Pooley, G. G., & Green, D. A. 1993, MNRAS, 264, L17
Richmond, M. W., et al. 1994, AJ, 107, 1022
Rybicki, G. B., & Hummer, D. G. 1991, A&A, 245, 171
Schmidt, B. P. 1993, Ph.D. thesis, Harvard Univ.
Schmidt, B. P., et al. 1994a, AJ, 107, 1444
Schmidt, B. P., et al. 1994b, ApJ, 432, 42
Schmidt, B. P., Kirshner, R., & Eastman, R. 1992, ApJ, 395, 366
Schurmann, S. 1983, ApJ, 267, 779
Swartz, D. 1991, ApJ, 373, 604
Tanaka, Y., et al. 1993, IAU Circ., No. 5753
Trammell, S., Hines, D., & Wheeler, J. C. 1993, ApJ, 414, L21
Utrobin, V. 1994, A&A, 281, L89
Van Dyk, S. D., Weiler, K. W., Sramek, R. A., Rupen, M. P., & Panagia, N. 1994, ApJ, 432, L115
Wheeler, J. C., & Filippenko, A. V. 1994, in Supernovae and Supernova Remnants, ed. R. McCray & Z. W. Li (Cambridge: Cambridge Univ. Press), in press
Woosley, S. E., Eastman, R., Weaver, T. A., & Pinto, P. 1994, ApJ, 429, 300
Zimmermann, H.-U., et al. 1994, Nature, 367, 621